University of Ljubljana
Faculty of Mathematics and Physics
Physics Department

Andrej Studen

Semiconductor drift detectors and their applications

Seminar

Adviser: prof. dr. Marko Mikuž

Abstract

Low production cost and small number of readout channels per unit area are two of the most prominent features of the semiconductor drift detectors. They are used in very diverse applications, from photon detection to fast particle tracking. This paper presents the principle of operation of a semiconductor drift device and lists two applications: the silicon vertex tracker of the STAR experiment and DEPFET structures to be used in a future X-ray satellite telescope.

Contents

1 Introduction

Semiconductors play an important role as detectors of high energy experiments. Their most prominent feature is detection of the tracks of the charged particles with spatial resolution down to 1 μm. As crystral structures, they are also robust and rigid and with small thicknesses (300 μm) the particle scatter is minimized. The most common position sensitive sensors used are either pad- or strip granulated detectors.

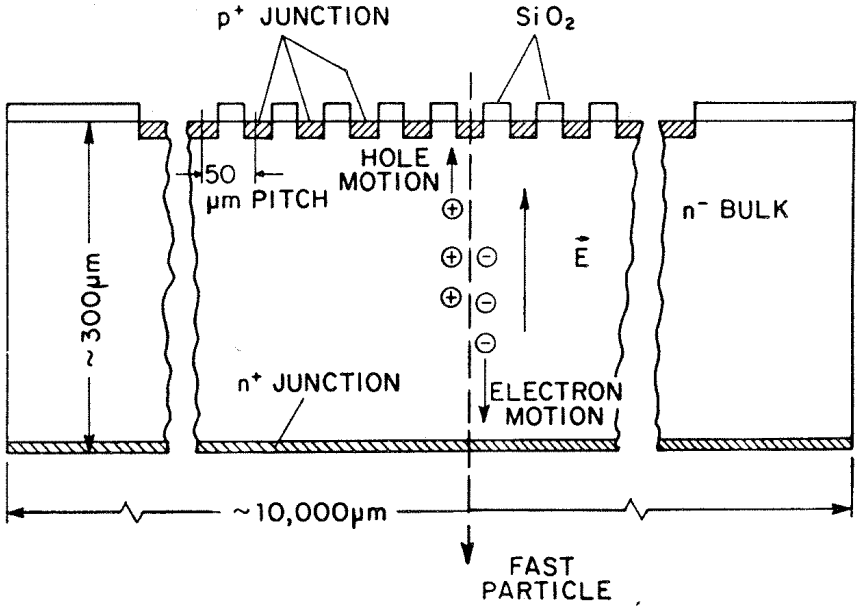

Figure 1: Schematic drawing of a standard single-sided semiconductor strip detector. Bulk is a moderatly doped semiconductor, with ohmic contact to the backplane electrode, achived through a highly doped layer of the same doping type as the bulk. The strips on the top side are electrodes with ohmic contact to highly doped semiconductor implants with opposite doping with respect to the bulk. With suitable potential (relative to the back-plane) applied to the front side, each strip serves as a reversly biased diode. In the space-charge region electron-hole pairs created by the traversing fast charged particle, are separated by the electric field and collected on the electrodes. After [1]

Fig. 1 shows an example of a single-sided micro-strip detector. The bulk is a moderatly, usually n-type ($N_D < 10^{18}$ m^{-3}) doped semiconductor. The potential of the bulk is defined through a highly doped ($N_D^+ \approx 10^{24}$ m^{-3}) semiconductor layer (n$^+$) of the same doping type which is in contact with a metal electrode. Other side of the wafer has highly doped ($N_A^+ \approx N_D^+$) semiconductor implants (p$^+$) in the form of strips with typical pitch of 40-80 μm. Doping is opposite to the bulk, so each strip serves as a diode. Reverse bias potential, $-U$ is applied to the p$^+$-n diodes so space-charge region depleted of charge carriers is created beneath the strips. The depletion region depth $d = \sqrt{2\varepsilon\varepsilon_0 U/e_0 N}$, with $\sqrt{2\varepsilon\varepsilon_0/e_0} = 363\ \mu\text{m} \times \sqrt{10^{18}\text{m}^{-3}/100V}$ depends on the densitiy of the doping atoms in the layer, N. Voltages of about 100 V (N dependent) deplete the bulk, while the depletion depth in the p$^+$ implants remains shallow (few nm). As the

fast charged particle passes through the semiconductor, deposited energy is converted to electron-hole pairs (about 22500 in 300 μm of silicon). In the space-charge region the electric field splits the electrons and the holes. A current pulse induced by moving carriers is obtained on the metalic contacts.

Position sensing in micro-strip detectors is obtained by granularity of the strip implants. Positioning along a single dimension (orthogonal to strips) can be done by the device described with a resolution of 5-10μm for the mentioned pitches. The number of readout channels per unit length for such resolution remains large (200 /cm) and poses a practical problem, specially for large devices. Semiconductor drift detectors (SDD) present an alternative, as one-dimenisonal positioning can be achieved via a single readout electrode with a similar spatial resolution.

First section is devoted to the presentation of the SDD. In the second part, application of the chambers for the STAR experiment at Brookhaven RHIC is described. Third part deals with an offspring of the SDD developement, a DEPFET, which combines principles of SDD with electronics to form a monolythic detector-amplification device.

2 Principles of operation for a SDD

To define the potential of the n-bulk of the wafer, n^+ implant does not need to extend over the whole wafer surface, as in Fig. 1, but can be smaller in size as well as positioned anywhere on the wafer. (We will always refer to the special case where the bulk is doped with donors (n-type). But with appropriate adjustments for doping types all the preceeding as well as all the following statements hold for p-bulk semiconductors as well.) Fig. 2 shows the depletion of a wafer with an electrode on a wafer side, far away from the profile drawn. We start with a simple semiconductor pn junction detector, with a p^+ layer on top, n-bulk and a n^+ contact on the bottom (p^+-n-n^+). Fig. 2(a) shows two such detectors, with both n^+ layers aligned and grounded. When small negative voltage is applied to p^+ layers on both detectors simultaneously, the space-charge area starts to grow from the p^+-n junctions in both detectors. The undepleted middle region is still conductive and at potential (ground) defined by the n^+ contacts. Even if n^+ layers are removed [Fig. 2(c):(top)] the conductive channel in the bulk center retains the potential of the electrode at the wafer side. So the potential profiles [Fig. 2(b),(c):(bottom)] are equal in both structures. When the potential difference is increased beyond the full depletion voltage $U_{FD} = e_0 N_D (l/2)^2 / 2\varepsilon\varepsilon_0$, where $e_0/2\varepsilon\varepsilon_0 = 7.6\ V \times 1/10^{18}\ \mathrm{m}^{-3} (100\ \mu\mathrm{m})^2$ in the structure without the n^+ layer and thickness l, the conductive channel in the bulk center disappears [Fig. 2(d):(right)] , while the potential profile across the wafer (coordinate x) obtains a parabolic profile [Fig. 2(d):(left)]. Any further increase of the bias voltage results in a parallel shift of the parabola. The center of the bulk is now at a potential minimum in the x direction for electrons, while holes are collected on the p^+ electrode on the device surface. We are free to shape the potential in other dimensions, as long as the bulk remains depleted. Linear potential drop in one of the directions, parallel to the surface, will sweep the electrons to the wafer side. Fig. 3 shows the potential gutter, realized with p^+ strips on top and the bottom side of the wafer attached to linearly varying potential. The adjacent strips only shift the parabola but retain the depletion of the bulk. The p^+ stirps are called field strips and the drift direction is

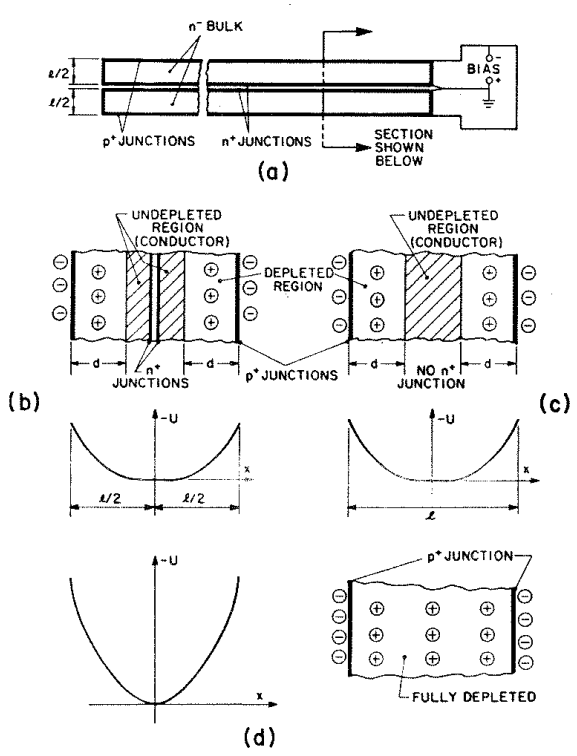

Figure 2: Principle of depletion of a semiconductor with electrode at the wafer side. (a) Two back to back p^+-n-n^+ diodes of thicknesses l/2 with n^+ layers on the same potential. (b) (top) application of the reverse bias to a two-diode structure from (a), (bottom) potential profile across the detector. (c) (top) application of reverse voltage to a semiconductor structure of thickness l with n-bulk doping and p^+-implants on both sides. Potential of the bulk is defined far away at the wafer side. Conductive channel serves as the connected n+ layers.(bottom) potential profile across the wafer. (d) Fully depleted wafer wtih p^+ junctions on both sides, (left) potential profile across the wafer and (right) the disappereance of the conductive channel [1].

orthogonal to the strips.

In mathematical terms, we are solving the Poisson equation for the semiconductor. We will discuss the solution in the abrupt junction approximation. That means that we neglect the signal currents and claim that all other currents are balanced so that net currents in the semiconductor are neglible. We also neglect built in and thermal potentials as they are indeed small when compared to external voltages applied. Then the Poisson equation for electro-static potential reads:

$$\nabla^2\varphi = -N_{\mathrm{D}}e_0/\varepsilon\varepsilon_0 \tag{1}$$

Linearity of operator ∇^2 allows one to write the solution in the form of $\varphi = \varphi_1 + \varphi_2$. Potential φ_1 has to solve the Poisson equation, $\nabla^2\varphi_1 = -N_{\mathrm{D}}e_o/\varepsilon\varepsilon_0$, while the second term must satisfy the Laplace equation $\nabla^2\varphi_2 = 0$. Different operating detectors give different solutions for the equations given.

2.1 Linear Drift Detectors

The biasing of this device is done with parallel field strips. We define the coordinate y to be the drift direction. For φ_1 we find 1D solution to the equation:

$$\frac{d^2\varphi_1}{dx^2} = -\frac{e_0N_{\mathrm{D}}}{\varepsilon\varepsilon_0} \tag{2}$$

as

$$\varphi_1 = -e_0N_{\mathrm{D}}/(2\varepsilon\varepsilon_0)(x - x_0)^2 + \varphi_0, \tag{3}$$

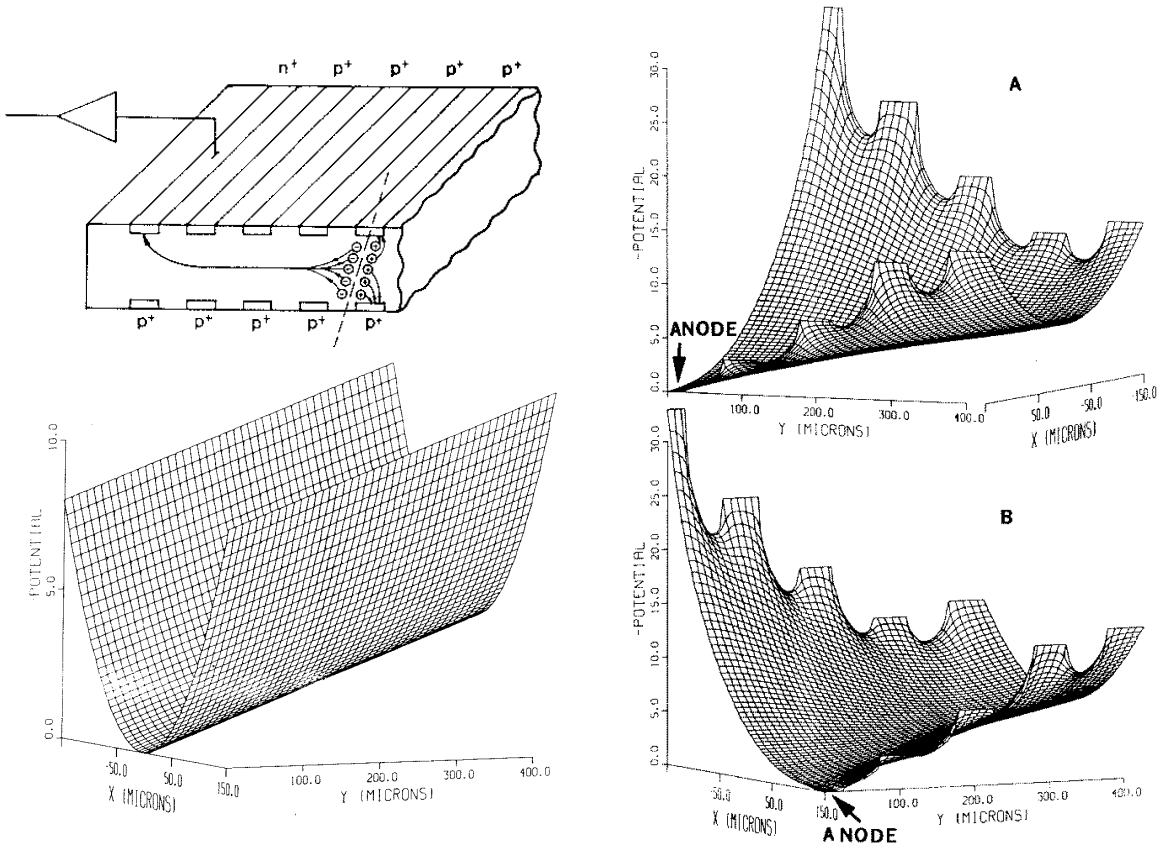

Figure 3: Top left: Schematic drawing of the track in a SDD. Electrons get collected on the anode, holes on the field electrodes. Bottom left: The electric potential of the linearly graded SDD, sketched above. Parabolic gutter sweeping the charges is shown. Right: simulation of the potential in a SDD, close to the anode. Linear region stops approx. 400 μm from the anode. In the proximity the potential gutter is shifted to the surface (x=150 μm) as less negative potential is applied to the field electrodes on the anode side of the wafer.

where x_0 (potential minimum depth) and φ_0 (potential offset) remain integration constants, dependent on the boundary conditions. The potential shown in Fig. 2(d) is a realization with x_0 at the bulk center. Solutions to the second equation have to be linear in all dimensions to satisfy the Laplace equation. Simple realization, shown in Fig. 3 is:

$$\varphi_2 = -E \cdot y \tag{4}$$

which can be achieved with linear strip potential dependence on the distance of the strip from the anode. Bending of the gutter towards the surface is achieved with non-equal potentials applied to the field strips on the opposite sides of the wafer, or in terms of the solution (*3*) shifting of the integration constant x_0. The anode can be thus placed on the top of the wafer.

Fig. 3 (right) shows a simulation of the potential in a strip semiconductor drift detector. Linear region stops approx. 400 μm away from the electrode. In the proximity

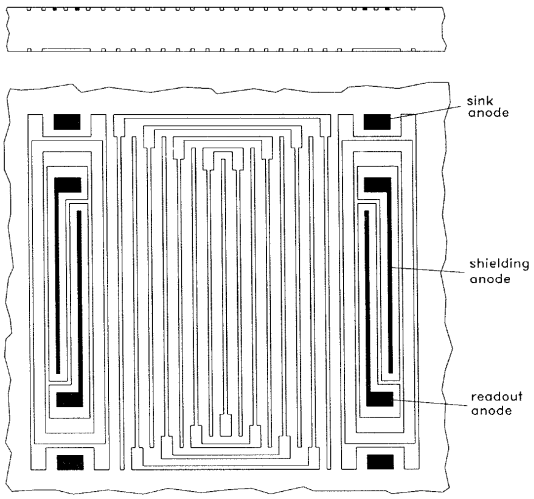

Figure 4: Schematic of a simple linear drift detector. Dark anodes are connected to n^+ implants, light field electrodes to p^+ implants. The carriers drift from the central field implant to the anodes. The shielding diode drains the electrons from the high voltage protection region, while the readout anode collects the signal.

of the anode, the p^+-n junctions on the anode side of the detector are biased less negatively than the junctions on the opposite side, so potential minimum shifts to the anode plane. Fig. 4 shows a top view of the schematic of a linear drift detector. Carriers drift away from the central field (p^+) implant which is at the most negative potential. Biasing of the field is done through polysilicon resistors line imbeded on the wafer or punch-through biasing, a single voltage connection is needed for the drift field formation. Together with the ground applied to the anode the biasing requires as many contacts ordinary strip sensors. Some of the field diodes are connected to the symmetrical strips at the same potential on the other side of the detector, forming a high-field protection region to provide controlled drop of the negative potential over the semiconductor bulk (top and bottom middle regions on Fig. 4). Anodes are shielded from each-other with p-implants, the outer electrode serving as a drain for the electrons from the high-field protection region.

Position sensing in linear drift detector is done with timing measurements of the signal with respect to reference trigger signal. Triggering can be done on the field diodes where the hole signal is collected [2], with a scintilator counter in particle beam[3] or some other signal. Drift velocity of the electrons is proportional to the constant drift field E (*4*) and allows one to reconstruct the position of interaction, y_{int} through signal arrival time, τ, as $y_{\text{int}} = \mu E \tau$, with μ the mobility of electrons. Fig. 5 shows the signals of a linear SDD, deposited by a light pulsar which also served as the trigger reference. For the left side of the figure, pulsar was positioned at various distances from the anode, so position sensitivity can be observed. On the right, different drift fields were applied, while the pulsar remained at a fixed position. Slow drift velocity may cause the spread of the signal [Fig. 5(i)] which may compromise the spatial resolution. Front-end electronics must be therefore adjusted for different drift velocities to obtain maximal spatial resolution [4].

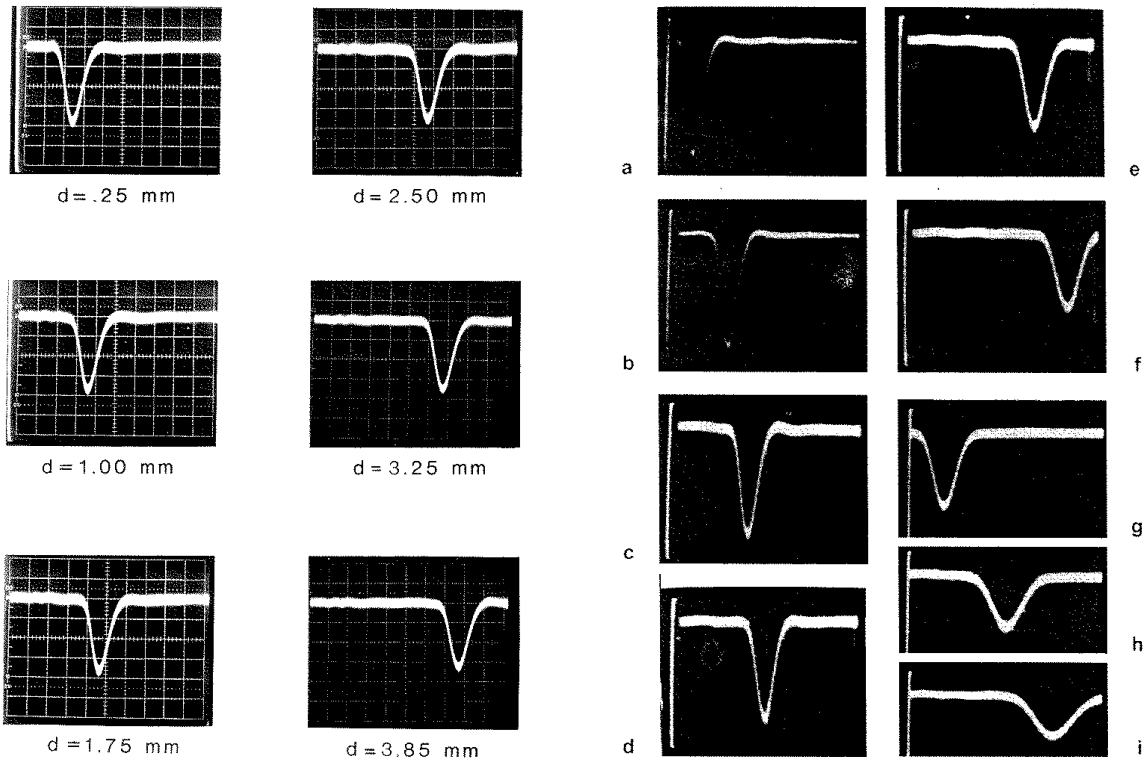

Figure 5: Amplified and shaped signal of a linear drift detector with constatn drift field, caused by a charge injection with a light pulser. After [3]. Left: signal shape for 6 different distances from anode shown. Time scale is 200 ns/div and the drift field is 265 V/cm. Right: signal shape for various field strengths: (a) 425, (b) 265, (c) 210, (d) 185, (e) 130, (f,g) 105, (h) 80 and (i) 67 V/cm. Time scale is 200 ns/div, horizontal scale is shifted f0r 0.4 μs in figutres from (g) to (i). The pulser was 3.5 mm away from the diode.

2.2 Matrix drift detectors

Matrix drift detectors are obtained by divison of the anode in the strip direction(z). The y coordinate is still read out by the timing properties of the signal, while the traverse (z) direction is given by the position of the read-out pad. Fig. 6 shows a matrix SDD, with dark readout anodes and light field electrodes. p-implants surround and hence insulate each of the readout anodes. From signal sharing among adjacent pads spatial resolution along the z-direction can be improved. Sharing between more than two pads can compromise the two-track resolution, so the signal spread [Fig. 5(i)] due to the diffusion and carrier repulsion can be controlled with special production techniques [5].

2.3 Radial Drift Detectors

With radial devices, the central anode can have extremely small capacitance and can therefore serve as a very precise spectrometer. Fig. 6 shows such a device. Charges drift to the center of the device, where small anode collects the signal. Capacitances of

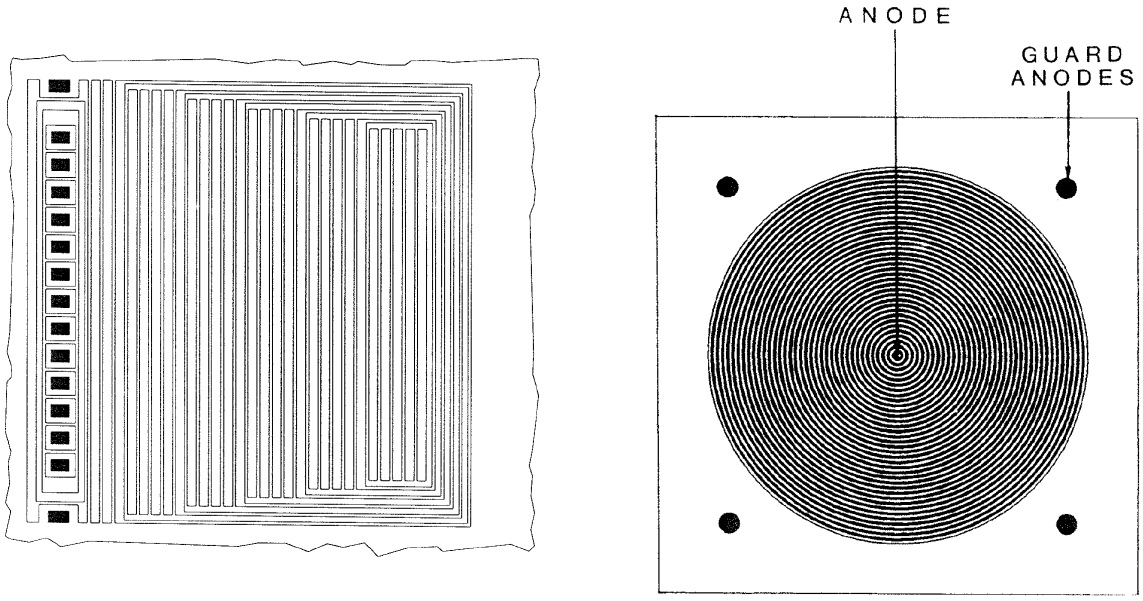

Figure 6: Left: Matrix SDD. The anodes are insulated with p-implants from each other. Right:Radial drift detector. Point anode of 200 μm in the center has small capacitance (0.1pF). [3]

Table 1: Comparison of detector parameters for strip detectors, SSD and charge coupled devices (CCD) [7, 8, 9]

	strip[ATLAS]	SDD[STAR]	CCD [XMM]
noise [e ENC]	1000	500	50
Readout time	25 ns	5 μs	5 ms
Readout channels per sensor	$\mathcal{O}$(2/p)	$\mathcal{O}$(1/p)	1
Spatial resolution [μm]	23	17	50-75

10-100 fF are reachable. Radial detectors with outward radial drift can also be realized and position sensing is obtained with segmentation of the anode ring on the outside rim of the device. With such a setup spatial resolution in the direction perpendicular to the radius ,r_ϕ for events close to the center of the device is excellent ($\Delta r_\phi = r\Delta\phi$). Such devices were used for CERES experiment at CERN [6].

3 STAR experiment

STAR epxeriment is one of the four experiments hosted on the Relativistic Heavy Ion Collider (RHIC) at the Brookhaven National Laboratory. The aim of the experiment is to observe the quark-gluon plasma (QGP). Very dense and hot nuclear matter is believed to enter the phase where quarks behave as free particles. This is the same stage that appeared 10^{-6} s after the Big-bang. Estimated duration of the QGP state is only 10^{-22} s before the hadronization occurs. The RHIC energy of 100 GeV/nucleus is believed to

be large enough to produce QGP in heavy ion (Au-Au) collisions. The separation of QGP from ordinary hadronic condensation is a tedious task. Suggested signatures of QGP are abundance of strangness [10] so devices identifying multi-strange baryons (Ω^- and Ξ^-) and ϕ mesons must be implemented. As this is not the only QGP signature, all other observables must be closely monitored. The time evolution of nucleus-nucleus collision involves several phases, so fast as well as slow particles need to be detected. Fig. 7

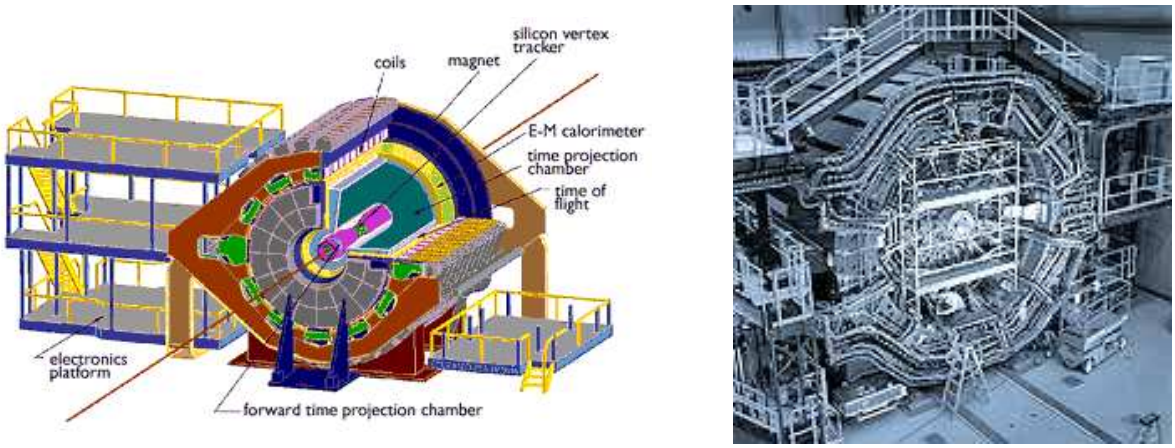

Figure 7: Left: diagram of the STAR experiment on RHIC of the BNL, sideview. Right: Photo of the side of the STAR detector.

shows a schematic of the STAR detector. The heart of the detector are the time projection chambers (TPC), which are large (2 m wide) drift chambers which track particles with traverse momenta $p_\perp$>150MeV/c, and do particle identification based on energy loss measurements. Silicon vertex detector (SVT) based on silicon drift chambers can improve the performance of the TPC significantly. First, as it is positioned close to the beam pipe [Fig. 7] it can track even short-lived particles, including multi-strange baryons invisible to the TPC. Second it can track particles with traverse momenta down to 40 MeV/c. And in addition it provides additional points for tracking reconstruction and particle identification [11]. SDD were choosen for their low cost, small number of readout channels and RHIC bunch-crossing times of 100 μs giving enough time to read out the whole detector. Fig. 8 shows a matrix SDD used in SVT of the STAR experiment. Semiconductor used was high resistivity (3 kΩcm) n-type silicon, with symmetric p-strips on both sides of the wafer, as shown in Fig. 6(left). The active area of the sensor is 6×6 cm^2. The pitch for the field electrodes is 120 μm, the anodes are segmented with the pitch of 250 μm. The central field electrode [Fig. 8] is nominaly on -1.5 kV potential with respect to the readout anode. This potential difference indicates drift fields of 500 V/cm or drift velocities of about 6.75 mm/μs [8]. The non-linearity of the drift field can be observed together with the corresponding position resolution on Fig. 9. Drift time for electrons created near the central field electrode is 4.5 μs which is smaller than the TPC readout time of 50 μs and the bunch crossing time of 100 μs. Resolution of 17 μm was measured along the drift direction [Fig. 9(c)] and 8 μm along the anode direction [Fig. 9(d)]. The SVT was installed in July 2001 and started to collect data.

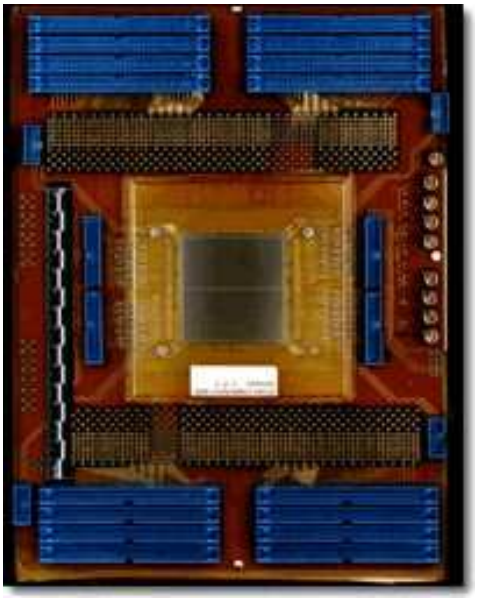

Figure 8: Left: top view of a SDD used for STAR SVD. Field strips are vertical, anodes are segmented and wire-bonded to the readout electronics on the hybrid. Right: Photo of the assembled SVD with physicists. Several sensors are assembled on a ladder with readout at the sides.

4 Depleted transistor applications in X-ray imaging

Measurements of X-ray spectra present a serious problem as the signal size is comparable to the noise threshold in many sensors. In semiconductors, X-rays are mostly photo-absorbed, and the scattered electron produces pairs of electrons and holes. For example, $K_{\alpha,1}$ line of iron (Fe) has the energy of 5.49 keV, and photon emitted from that state produces 1520 electron-hole pairs in silicon. With suitable electric field charges can be collected on the readout electrodes, connected to a charge sensitive amplifier. Noise at the amplifier input is linearly dependent on the capacitive load, so low capactive coupling of the input line to the surrounding electrodes is desired. With sidewards depletion, presented in section 2, anodes can be made very small so their capacitance can be of order of 10-100 fF [6]. Additional traces carrying the signal as well as wire bonds would add significantly to the input capacitance (1 pF/cm), so amplification at the detection point is desired. One of the first hybrid sensors where amplification is embeded in the device are fully depleted transistors. With low capacitance described they are ideal sensors for X-rays.

Fig. 10 shows the concept of a DEPMOS, a fully deplleted p-channel MOSFET. It is a combination of the MOSFET (b) with a sidewards depletion concept (a). Proposed design (c) has a potential minimum for the signal electrons located close to the transistor region of the sensor in the n-bulk. Biasing is done through the clear electrode and the p^+ implants. Passing particle deposits electron-hole pairs, which are separated by the depletion field. Holes drift to the p^+ implants, electrons are gathered in the potential well below the gate. They induce charges in the inversion layer of the MOS structure and the transistor source-to-drain current is proportional to the charge collected in

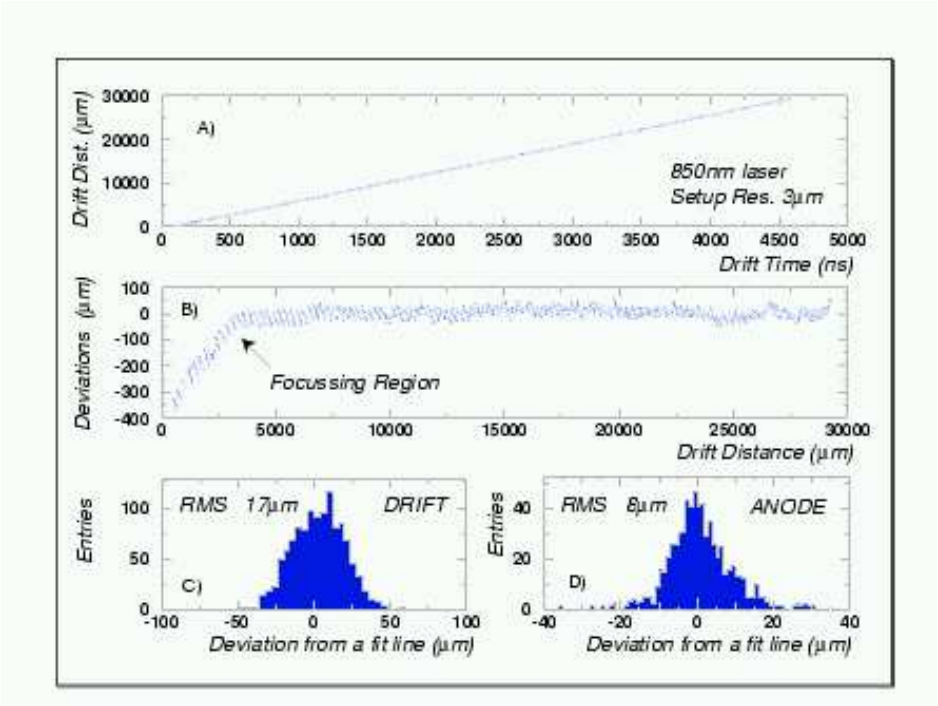

Figure 9: (a) Measurement of the drift time of the SDD used in SVT with a laser. (b) Deviation from linear drift.(c) Histogram of differences between data points and the straight line, resolution in the drift direction.(d) Histogram of differences between the actual and the reconstructed position of laser injection hit in anode direction. After [8].

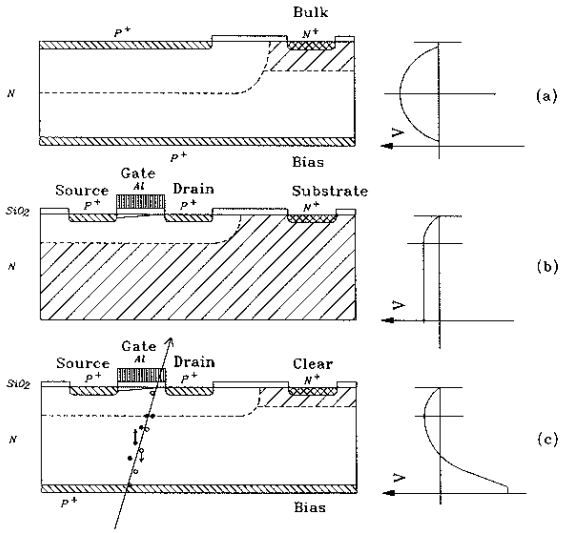

Figure 10: Conceptual design of DEPMOS. Dashed lines show potential minima for electrons, hatched areas are undepleted. Potential across the wafer is sketched on the right. (a) shows an ordinary drift detector, with N^+ anode supplying potential to the bulk and P^+ depleting the bulk. (b) sketches a MOSFET. Gate is as MOSFET structure. Source and drain are asymmetrically doped p-implants. (c) a DEPMOS sensor. Clear acts as the anode of SDD.

the well. With suitable biasing scheme the potential close to the transistor part in DEPMOS can be made similar to that of the ordinary MOSFET to retain its performance [Fig. 10]. Potential well in the drift direction is formed through partial compensation of the surface doping of source and drain implants resulting in a potential minimum

below the gate electrode [4]. Positive potential applied to the clear electrode breaks this potential minimum so trapped electrons can be removed when desired. Positive pulses applied occasionally will also remove thermaly excited electrons from the well.

Figure 11: The XEUS X-ray satellite telescope to be launched in 2010. Two separate spacecrafts will simulate a telescope with focal length of 50 m [12].

Fig. 11 shows a proposed X-ray satellite telescope [9]. It will replace the currently operating XMM detector, extending its sensitivity by the factor of 100. Two separate spacecrafts will be launched with a single Ariane V, the Mirror spacecraft(MSC) and the Detector spacecraft(DSC). The relative position of the pair will be adjusted to 1 mm so focusing at the distance of 50 m will be maintained. The effective collection area of the mirror is 6 m^2, and two docking ports on the MSC will enable joint rendez vous with the International Space Station for refurbishing and expansion.

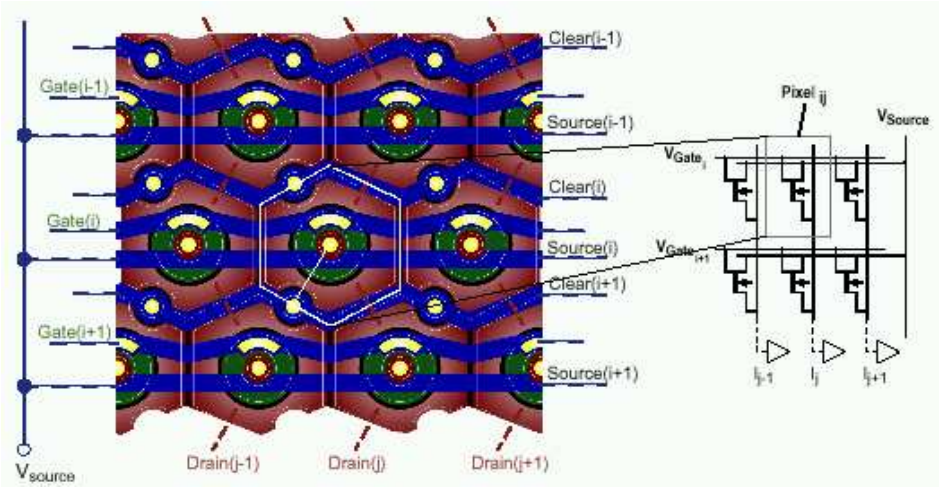

Figure 12: DEPFET pixel matrix designed for XEUS mission. The dashed white line indicates the outline of a single pixel. Dark (red) lines are the connections of the drains.

One of the instruments on the DSC will be the Wide Field Imager. Sensors will have to cover a 7×7 cm^2 large area, with small pixel size (50 μm)^2, provide reasonable readout time and avoid "out of time" events. Detection of photons from 150 eV to 30 keV is demanded. The requirements can be met with a deep p-channel FET (DEPFET) pixel matrix detector. Fig. 12 shows the pixel design of the device. It is constructed of 1024× 1024 pixels with 50 to 75 μm pitch, total area covering 76×76 mm^2.

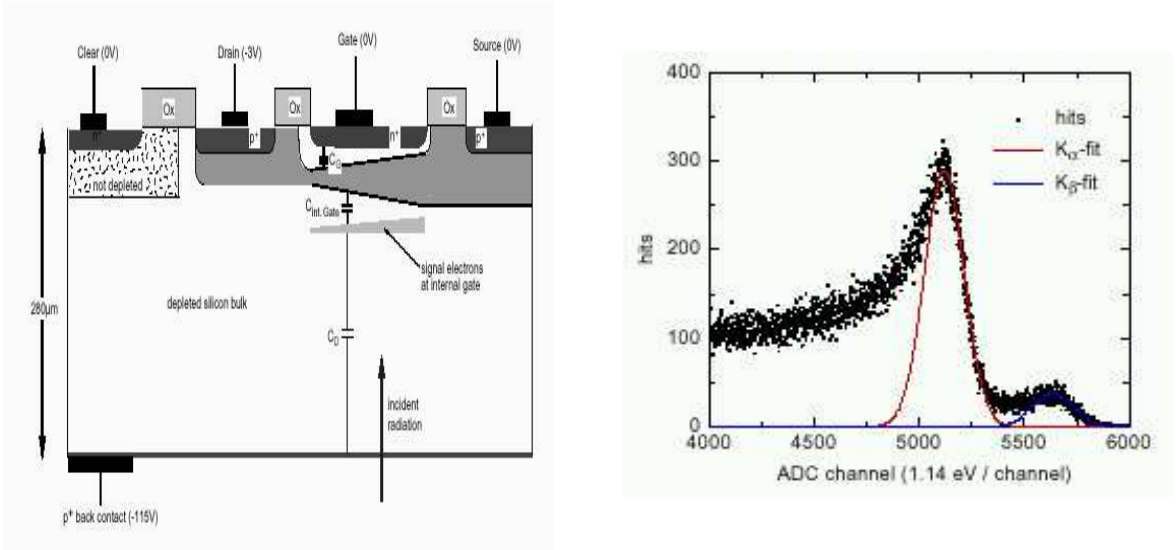

Figure 13: Left: schematic cross-section (see Fig.12) of a single DEPFET pixel. Voltages used for the readout phase shown.

Fig. 13 (left) shows the cross-section of a pixel. Transistor is realized on a high ohmic n silicon bulk, with circular source p^+ implant, surronded by the n^+ gate embeded in the p^+ drain. High energy implants serve as p-channel connecting source and drain. Suitablly biased backplane and surface p^+ implants create a potential well for the electrons in the bulk below the gate. Electrones produced by incident radiaton during integration time are collected in the well (internal gate). Positive potential on the gate insulates the source from the drain. During read-out time positive voltage on the gate is cleared and the charges collected modulate the transistor current. The readout can be repeated as the charges remain trapped (non-destructive readout). Third stage is the clear stage. With positive pulses applied to the clear contact, potential well diminishes and charges are sweept to the clear anode. Fig. 13 shows the collected X-ray spectra of ^{55} Fe with K_α and K_β Mn lines. The room-temperature resolution is esitmated by the fit and gives incredible 158 eV (12 e ENC) noise on the peak. The large tail to the lower energy is the charge sharing contribution due to the small pixel size. Threshold was estimated at 200 eV.

5 Summary

Silicon drift detectors were shown to be a useful device in wide spectra of detection applications. They are based on the ingenius idea of side-depletion of the bulk. Readout of one dimension can be done in a linear drift detector with a single readout anode. Two-dimensional readout is realized with the segmentation of the anodes and can be done in either matirx (square) or radial form. The STAR experiment uses silicon drift detectors for SVT. Characterization of the detectors shows the position resolution of 17 μm, comparable to the resolution of the silicon micro-strip detectors. Amplification can be integrated on a sensor with the sidewards depletion principle, as it is done in

fully depleted transistors. XEUS mission will rely on a DEPFET matrix detector to detect X-ray radiation. Resolution of the devices was measured to be 158 eV FWHM at the room temperature on the ^{55}Fe K_α line.

References

[1] E. Gatti and P. Rehak. "Semiconductor Drift Chamber-An Application of a Novel Charge Transport Scheme". *Nucl. Inst. Meth.*, pages 608–14, **225** (1984).

[2] P. Rehak, J. Walton, E. Gatti, et al. "Progress in Semiconductor Drift Detectors". *Nucl. Inst. Meth.*, pages 367–78, **A248** (1986).

[3] E. Gatti, P. Rehak, et al. "Semiconductor Drift Chambers". *IEEE Trans. Nucl. Sci.*, pages 1204–8, **32** (1985).

[4] G. Lutz. *"Semiconductor Radiation Detectors"*. Springer, (1999).

[5] A. Castoldi, P. Rehak, and P. Holl. "A new Silicon Drift Detector with Reduced Lateral Diffusion". *Nucl. Inst. Meth.*, pages 375–80, **A377** (1996).

[6] W. Chen, H. Kraner, Z. Li, et al. "Performance of the Multianode Cylindrical Silicon Drift Detector in the CERES NA45 Experiment: First Results". *Nucl. Inst. Meth.*, pages 273–8, **A326** (1993).

[7] H. Pernegger. "Recent Test Results for ATLAS SCT Modules". http://ltp.web.psi.ch/VERTEX2001/. presented at the VERTEX 2001 workshop.

[8] D. Lynn, R. Bellwied, R. Beutenmueller, et al. "The STAR Silicon Vertex Tracker: A Large Area Silicon Drift Detector". http://www.star.bnl.gov. talk presented at the VERTEX 99 Workshop.

[9] P. Fischer P. Holl, P. Klein, et al. "Active Pixel Matrix for X-ray Satellite Missions". *IEEE Trans. Nucl. Sci.*, **47**(2000) 4.

[10] J. Rafelski, G. Torrieri, and J. Letessier. "The Strange Quark Gluon Plasma". http://arXiv.org/ps/nucl-th/0101025. presented at the 6th Interantional Workshop on Relativistic Aspects of Nuclear Physics.

[11] R. Beutenmueller, W. Chen, D. DiMassimo, et al. "Proposal for a Silicon Vertex Tracker (SVT) as an Upgrade for the STAR Experiment at RHIC". http://www.star.bnl.gov.

[12] G. Lutz. "Silicon Pixel-Detectors for the X-ray Astronomy". http://ltp.web.psi.ch/VERTEX2001/. presented at the VERTEX 2001 workshop.